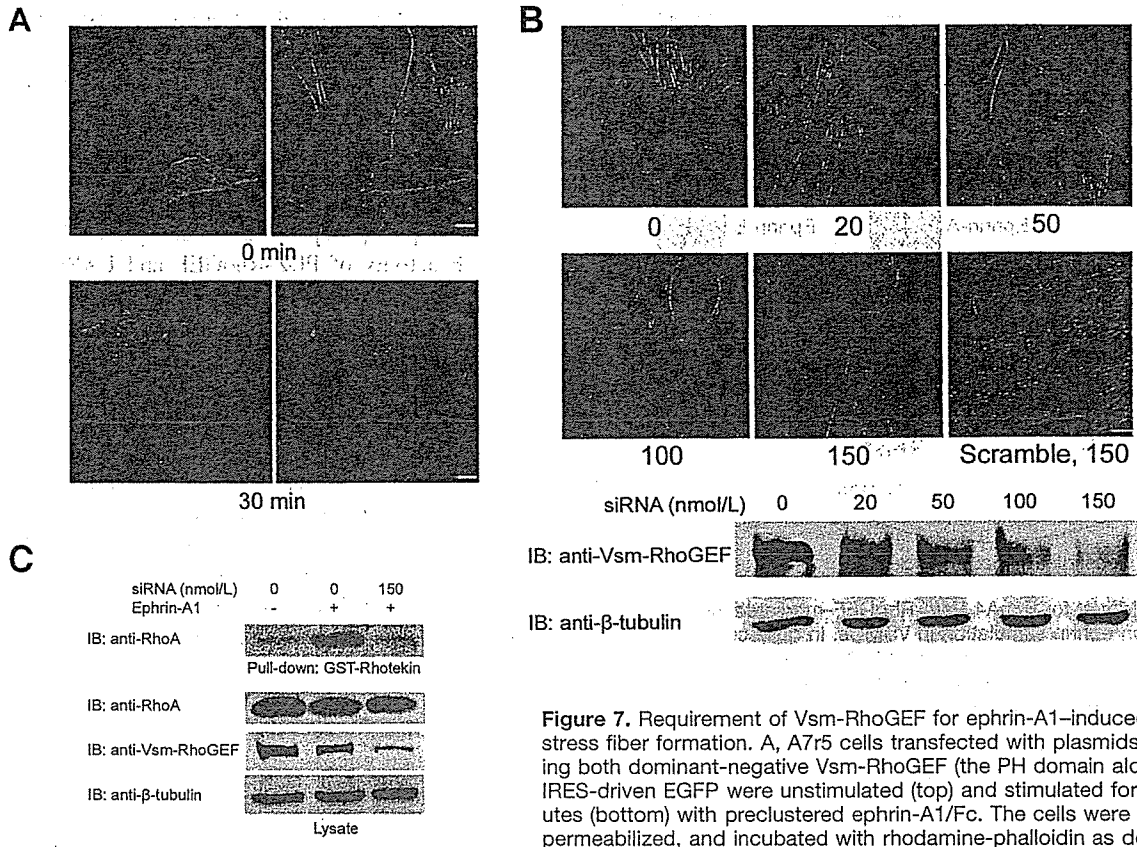

Figure 7. Requirement of Vsm-RhoGEF for ephrin-A1–induced actin stress fiber formation. A, A7r5 cells transfected with plasmids expressing both dominant-negative Vsm-RhoGEF (the PH domain alone) and IRES-driven EGFP were unstimulated (top) and stimulated for 30 minutes (bottom) with preclustered ephrin-A1/Fc. The cells were fixed, permeabilized, and incubated with rhodamine-phalloidin as described in the legend of Figure 5B. Bar=20 μm. B, A7r5 cells transfected with Vsm-RhoGEF–specific small-interference RNA (siRNA) or with scrambled siRNA for 24 hours at the concentration (nmol/L) indicated at the bottom. The assembly of actin stress fiber in the cells was visualized as in panel A (top). The lysates of A7r5 cells transfected with Vsm-RhoGEF siRNA at the concentration as indicated at the top were subjected to immunoblot with either anti-Vsm-RhoGEF or anti-tubulin as an internal control (bottom). Bar=20 μm. C, A7r5 cells untransfected or transfected with Vsm-RhoGEF siRNA were unstimulated or stimulated with ephrin-A1 as indicated at the top and analyzed for GTP-bound RhoA using pull-down assay. Cell lysates were subjected to SDS-PAGE, followed by immunoblot analysis using antibodies as indicated at the left.

interference RNA specific to Vsm-RhoGEF exhibited less actin stress fiber and became shrunken, which paralleled the reduction of Vsm-RhoGEF (Figure 7B). Furthermore, A7r5 depleted of Vsm-RhoGEF did not show the increase in GTP-bound RhoA upon ephrin-A1 stimulation. These results indicate that Vsm-RhoGEF is required for ephrin-A1–dependent RhoA activation, which is a prerequisite for regulating actin stress fiber in A7r5 cells.

Discussion

RhoA is involved in Ca^{2+}-independent vascular smooth muscle contraction via Rho-kinase.[1] Most circulating vasoconstrictives, including angiotensin II, endothelin, and vasopressin, are suggested to induce smooth muscle contraction partly in a Ca^{2+}-independent Rho–Rho-kinase–dependent manner via $G_{12/13}$ and partly in a Ca^{2+}-dependent manner via $G_{q/11}$.[24] We demonstrated in the present study a novel Rho activation pathway triggered by the ephrin-A1–EphA4 interaction, which induces Vsm-RhoGEF phosphorylation in VSMCs.

Ephrin-Eph signaling is required not only for embryonic vascular development but also for angiogenesis by modulating endothelial cell migration and/or proliferation.[25,26] We have previously demonstrated that human aortic endothelial cells express EphB1 and that EphB1 activation causes membrane ruffling, a hallmark of increased cell motility.[16] Steinle et al[15] reported that EphB4 activation upon ephrin-B2 stimulation promotes endothelial cell migration via phosphatidylinositol 3-kinase. Conversely, ephrin-B1 upon EphB1 stimulation is shown to trigger angiogenesis, which was demonstrated by a corneal angiogenesis assay.[26] These data implicate the Eph-ephrin system in the regulation of vasculature. To date, only two reports demonstrated that ephrin-B2 is expressed in arterial vascular smooth muscle[27,28]; however, the physiological function of the Eph-ephrin system in VSMCs is unknown. We have shown for the first time that EphA4 is expressed in VSMCs in addition to vascular endothelial cells. Furthermore, we have found that an EphA4-associating molecule, Vsm-RhoGEF/KIAA0915, is specifically expressed in VSMCs.

We found that Vsm-RhoGEF associates with EphA4. Since ephexin, structurally related to Vsm-RhoGEF, contains DH and PH domains and associates with EphA4, we tested whether the DH and PH domains of Vsm-RhoGEF were required for its association with EphA4.[17] Both DH and PH domains of Vsm-RhoGEF are necessary for its association with EphA4, as shown in Figure 1. Previously, an intramolecular interaction of PH domain and DH domain has been

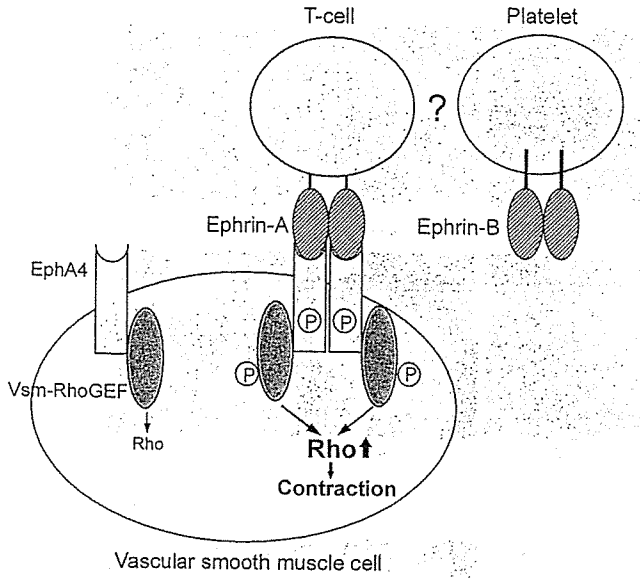

Figure 8. Model for EphA4-Vsm-RhoGEF–mediated RhoA activation upon ephrin stimulation in VSMCs. In quiescent cells, Vsm-RhoGEF associated with EphA4 affects basal contraction via RhoA irrespective of ephrin. Upon ephrin-EphA4 interaction triggered by cell-cell contact including T lymphocyte–VSMC and platelet–VSMC, EphA4 becomes autophosphorylated and induces tyrosine phosphorylation of Vsm-RhoGEF and the subsequent enhancement of GEF activity for RhoA, thereby inducing vascular smooth muscle contraction.

shown in Vav, one of the RhoGEF family members.[29] This intramolecular folding of DH and PH domains may occur and be required for the association of Vsm-RhoGEF with EphA4. Indeed, overexpression on the PH domain of Vsm-RhoGEF perturbed the association with EphA4 (Figure 1D). The PH domain alone functioned as a dominant-negative peptide, as shown in Figure 7A. PH domain functions as a membrane-targeting domain by binding to phosphoinositides.[30] Thus, overexpression of the PH domain might inhibit the membrane recruitment of Vsm-RhoGEF for activating RhoA (Figure 7A).

In this study, we observed that preclustered ephrin-A1/Fc chimera could induce EphA4 phosphorylation and subsequent signaling, leading to RhoA activation. It is unknown what cells contact VSMCs to trigger the ephrin-Eph interaction in normal and pathological conditions such as atherosclerosis and thrombosis. Candidate cells such as platelets and T lymphocytes have been shown to express ephrin-B1 and ephrin-A4, respectively.[31,32] Macrophages, T lymphocytes, and mast cells invade atherosclerotic lesions and may directly contact VSMCs.[33] VSMCs directly contact activated platelets at the site of thrombosis because the endothelial cell–VSMC contact is lost in the thrombotic region. This heterotypic platelet-VSMC contact may function in the pathological conditions to activate ephrin-Eph interactions. Furthermore, soluble ephrin-A4 has been found to be secreted from activated lymphocytes.[32] Thus, lymphocytes in atherosclerotic lesions may affect the contraction of VSMCs by direct contact and/or secretion of soluble ephrin-A4. Since vascular endothelial cells express ephrin-B1, the endothelial cell–VSMC contact may contribute to the regulation of vascular smooth muscle tone in normal conditions.

Vsm-RhoGEF functioned as a GEF for Rho and regulated actin stress fiber formation in VSMCs. Vsm-RhoGEF activity depends on its tyrosine phosphorylation, as shown in Figure 5A. Stimulation with preclustered ephrin-A1/Fc induces the phosphorylation of both EphA4 and Vsm-RhoGEF, thereby increasing the GEF activity of Vsm-RhoGEF. We previously reported that the activity of C3G, a GEF for Rap1, is increased upon phosphorylation at Tyr504.[34] Furthermore, the GEF activity of PDZ-RhoGEF and LARG, which link $G_{12/13}$ to RhoA, is enhanced by tyrosine phosphorylation by nonreceptor tyrosine kinases, FAK and Tec, respectively.[35,36] Thus, the tyrosine phosphorylation–dependent regulation of Vsm-RhoGEF is similar to other GEFs.

We observed that the reduction of Vsm-RhoGEF expression in A7r5 cells using RNA interference resulted in cell shrinkage and less stress fiber formation. These results suggested that basal RhoA activity regulated by Vsm-RhoGEF contributes to the maintenance of cell shape by regulating stress fiber formation and/or focal adhesion assembly.[11] Vsm-RhoGEF–regulated RhoA activity may also control basal muscular contractility by modulating the phosphorylation of both MLC and MLCP via Rho-kinase in vascular smooth muscle.[1] To address this issue, it will be interesting to see the phenotype of Vsm-RhoGEF gene-disrupted mice.

In conclusion, we have demonstrated a novel RhoA regulatory signaling pathway in VSMCs. Ephrin triggers EphA4-Vsm-RhoGEF–mediated RhoA activation in VSMCs. The GEF activity of Vsm-RhoGEF depends on its tyrosine phosphorylation after ephrin-A1–mediated EphA4 tyrosine phosphorylation (Figure 8). These results suggest that the EphA4-Vsm-RhoGEF-RhoA pathway may play a role in the regulation of blood pressure, atherogenesis, and thrombosis-triggered spasm.

Acknowledgments

This work was supported in part by grants from the Ministry of Health, Labor, and Welfare Foundation of Japan, from the Promotion of Fundamental Studies in Health Science of the Organization for Pharmaceutical Safety and Research of Japan, from the Ministry of Education, Science, Sports and Culture of Japan, from the Takeda Science Foundation Memorial, and from the Uehara Memorial Foundation. We thank Masamitsu Tanaka and Michiyuki Matsuda for the plasmids; Howard K. Surks for his critical comments; and Manami Sone and Hitomi Shimamoto for their technical assistance.

References

1. Somlyo AP, Somlyo AV. Signal transduction by G-proteins, Rho-kinase and protein phosphatase to smooth muscle and non-muscle myosin II. *J Physiol.* 2000;522(pt 2):177–185.
2. Kimura K, Ito M, Amano M, Chihara K, Fukata Y, Nakafuku M, Yamamori B, Feng J, Nakano T, Okawa K, Iwamatsu A, Kaibuchi K. Regulation of myosin phosphatase by Rho and Rho-associated kinase (Rho-kinase). *Science.* 1996;273:245–248.
3. Amano M, Ito M, Kimura K, Fukata Y, Chihara K, Nakano T, Matsuura Y, Kaibuchi K. Phosphorylation and activation of myosin by Rho-associated kinase (Rho-kinase). *J Biol Chem.* 1996;271:20246–20249.
4. Masumoto A, Mohri M, Shimokawa H, Urakami L, Usui M, Takeshita A. Suppression of coronary artery spasm by the Rho-kinase inhibitor fasudil in patients with vasospastic angina. *Circulation.* 2002;105:1545–1547.
5. Kandabashi T, Shimokawa H, Mukai Y, Matoba T, Kunihiro I, Morikawa K, Ito M, Takahashi S, Kaibuchi K, Takeshita A. Involvement of Rho-kinase in agonists-induced contractions of arteriosclerotic human arteries. *Arterioscler Thromb Vasc Biol.* 2002;22:243–248.

6. Bar-Sagi D, Hall A. Ras and Rho GTPases: a family reunion. *Cell.* 2000;103:227–238.
7. Scherer EQ, Herzog M, Wangemann P. Endothelin-1–induced vasospasms of spiral modiolar artery are mediated by Rho-kinase–induced Ca^{2+} sensitization of contractile apparatus and reversed by calcitonin gene-related peptide. *Stroke.* 2002;33:2965–2971.
8. Sauzeau V, Le Mellionnec E, Bertoglio J, Scalbert E, Pacaud P, Loirand G. Human urotensin II–induced contraction and arterial smooth muscle cell proliferation are mediated by RhoA and Rho-kinase. *Circ Res.* 2001; 88:1102–1104.
9. Hart MJ, Jiang X, Kozasa T, Roscoe W, Singer WD, Gilman AG, Sternweis PC, Bollag G. Direct stimulation of the guanine nucleotide exchange activity of p115 RhoGEF by $G\alpha_{13}$. *Science.* 1998;280: 2112–2114.
10. Fukuhara S, Chikumi H, Gutkind JS. Leukemia-associated Rho guanine nucleotide exchange factor (LARG) links heterotrimeric G proteins of the G_{12} family to Rho. *FEBS Lett.* 2000;485:183–188.
11. Etienne-Manneville S, Hall A. Rho GTPases in cell biology. *Nature.* 2002;420:629–635.
12. Eph Nomenclature Committee. Unified nomenclature for Eph family receptors and their ligands, the ephrins. *Cell.* 1997;90:403–404.
13. Wang HU, Chen ZF, Anderson DJ. Molecular distinction and angiogenic interaction between embryonic arteries and veins revealed by ephrin-B2 and its receptor Eph-B4. *Cell.* 1998;93:741–753.
14. Adams RH, Klein R. Eph receptors and ephrin ligands: essential mediators of vascular development. *Trends Cardiovasc Med.* 2000;10: 183–188.
15. Steinle JJ, Meininger CJ, Forough R, Wu G, Wu MH, Granger HJ. Eph B4 receptor signaling mediates endothelial cell migration and proliferation via the phosphatidylinositol 3-kinase pathway. *J Biol Chem.* 2002;277:43830–43835.
16. Nagashima K, Endo A, Ogita H, Kawana A, Yamagishi A, Kitabatake A, Matsuda M, Mochizuki N. Adaptor protein Crk is required for ephrin-B1-induced membrane ruffling and focal complex assembly of human aortic endothelial cells. *Mol Biol Cell.* 2002;13:4231–4242.
17. Shamah SM, Lin MZ, Goldberg JL, Estrach S, Sahin M, Hu L, Bazalakova M, Neve RL, Corfas G, Debant A, Greenberg ME. EphA receptors regulate growth cone dynamics through the novel guanine nucleotide exchange factor ephexin. *Cell.* 2001;105:233–244.
18. Niwa H, Yamamura K, Miyazaki J. Efficient selection for high-expression transfectants with a novel eukaryotic vector. *Gene.* 1991;108: 193–199.
19. Endo A, Nagashima K, Kurose H, Mochizuki S, Matsuda M, Mochizuki N. Sphingosine 1-phosphate induces membrane ruffling and increases motility of human umbilical vein endothelial cells via vascular endothelial growth factor receptor and CrkII. *J Biol Chem.* 2002;277: 23747–23754.
20. Northcott CA, Poy MN, Najjar SM, Watts SW. Phosphoinositide 3-kinase mediates enhanced spontaneous and agonist-induced contraction in aorta of deoxycorticosterone acetate-salt hypertensive rats. *Circ Res.* 2002;91: 360–369.
21. Okada Y, Sawa H, Endo S, Orba Y, Umemura T, Nishihara H, Stan AC, Tanaka S, Takahashi H, Nagashima K. Expression of JC virus agnoprotein in progressive multifocal leukoencephalopathy brain. *Acta Neuropathol (Berl).* 2002;104:130–136.
22. Kobayashi S, Shirai T, Kiyokawa E, Mochizuki N, Matsuda M, Fukui Y. Membrane recruitment of DOCK180 by binding to PtdIns(3,4,5)P3. *Biochem J.* 2001;354:73–78.
23. Reid T, Furuyashiki T, Ishizaki T, Watanabe G, Watanabe N, Fujisawa K, Morii N, Madaule P, Narumiya S. Rhotekin, a new putative target for Rho bearing homology to a serine/threonine kinase, PKN, and rhophilin in the Rho-binding domain. *J Biol Chem.* 1996;271:13556–13560.
24. Gohla A, Schultz G, Offermanns S. Role for G_{12}/G_{13} in agonist-induced vascular smooth muscle cell contraction. *Circ Res.* 2000;87:221–227.
25. Adams RH, Wilkinson GA, Weiss C, Diella F, Gale NW, Deutsch U, Risau W, Klein R. Roles of ephrinB ligands and EphB receptors in cardiovascular development: demarcation of arterial/venous domains, vascular morphogenesis, and sprouting angiogenesis. *Genes Dev.* 1999; 13:295–306.
26. Huynh-Do U, Vindis C, Liu H, Cerretti DP, McGrew JT, Enriquez M, Chen J, Daniel TO. Ephrin-B1 transduces signals to activate integrin-mediated migration, attachment and angiogenesis. *J Cell Sci.* 2002;115: 3073–3081.
27. Gale NW, Baluk P, Pan L, Kwan M, Holash J, DeChiara TM, McDonald DM, Yancopoulos GD. Ephrin-B2 selectively marks arterial vessels and neovascularization sites in the adult, with expression in both endothelial and smooth-muscle cells. *Dev Biol.* 2001;230:151–160.
28. Shin D, Garcia-Cardena G, Hayashi S, Gerety S, Asahara T, Stavrakis G, Isner J, Folkman J, Gimbrone MA Jr, Anderson DJ. Expression of ephrinB2 identifies a stable genetic difference between arterial and venous vascular smooth muscle as well as endothelial cells, and marks subsets of microvessels at sites of adult neovascularization. *Dev Biol.* 2001;230:139–150.
29. Das B, Shu X, Day GJ, Han J, Krishna UM, Falck JR, Broek D. Control of intramolecular interactions between the pleckstrin homology and Dbl homology domains of Vav and Sos1 regulates Rac binding. *J Biol Chem.* 2000;275:15074–15081.
30. Whitehead IP, Lambert QT, Glaven JA, Abe K, Rossman KL, Mahon GM, Trzaskos JM, Kay R, Campbell SL, Der CJ. Dependence of Dbl and Dbs transformation on MEK and NF-κB activation. *Mol Cell Biol.* 1999; 19:7759–7770.
31. Prevost N, Woulfe D, Tanaka T, Brass LF. Interactions between Eph kinases and ephrins provide a mechanism to support platelet aggregation once cell-to-cell contact has occurred. *Proc Natl Acad Sci U S A.* 2002;99:9219–9224.
32. Aasheim HC, Munthe E, Funderud S, Smeland EB, Beiske K, Logtenberg T. A splice variant of human ephrin-A4 encodes a soluble molecule that is secreted by activated human B lymphocytes. *Blood.* 2000;95:221–230.
33. Libby P. Inflammation in atherosclerosis. *Nature.* 2002;420:868–874.
34. Ichiba T, Hashimoto Y, Nakaya M, Kuraishi Y, Tanaka S, Kurata T, Mochizuki N, Matsuda M. Activation of C3G guanine nucleotide exchange factor for Rap1 by phosphorylation of tyrosine 504. *J Biol Chem.* 1999;274:14376–14381.
35. Chikumi H, Fukuhara S, Gutkind JS. Regulation of G protein-linked guanine nucleotide exchange factors for Rho, PDZ-RhoGEF, and LARG by tyrosine phosphorylation: evidence of a role for focal adhesion kinase. *J Biol Chem.* 2002;277:12463–12473.
36. Suzuki N, Nakamura S, Mano H, Kozasa T. Gα12 activates Rho GTPase through tyrosine-phosphorylated leukemia-associated RhoGEF. *Proc Natl Acad Sci U S A.* 2003;100:733–738.

Quasi-monochromatic parallel flash radiography achieved with a plane-focus x-ray tube

Eiichi Sato[a], Rudolf Germer[b], Yasuomi Hayasi[c], Etsuro Tanaka[d], Hidezo Mori[e], Toshiaki Kawai[f], Tatsumi Usuki[g], Koetsu Sato[g], Haruo Obara[h], Masayuki Zuguchi[h], Toshio Ichimaru[i], Hidenori Ojima[j], Kazuyoshi Takayama[j] and Hideaki Ido[k]

[a] Department of Physics, Iwate Medical University, 3-16-1 Honchodori, Morioka 020-0015, Japan
[b] ITP, FHTW FB1 and TU-Berlin, Blankenhainer Str. 9, D 12249 Berlin, Germany
[c] Electrical Engineering, Hachinohe National College of Technology, 16-1 Tamonoki Uwanotai, Hachinohe 039-1104, Japan
[d] Department of Physiology, School of Medicine, Tokai University, Boseidai, Isehara 259-1193, Japan
[e] Department of Cardiac Physiology, National Cardiovascular Center Research Institute, 5-7-1 Fujishirodai, Suita, Osaka 565-8565 Japan
[f] Electron Tube Division #2, Hamamatsu Photonics Inc., 314-5 Shimokanzo, Toyooka Village, Iwata-gun 438-0193, Japan
[g] Toreck Inc., 5-6-20 Tsunashima Higashi, Yokohama 223-0052, Japan
[h] Department of Radiological Technology, College of Medical Science, Tohoku University, 1-1 Seiryocho, Sendai 980-0872, Japan
[i] Department of Radiological Technology, School of Health Sciences, Hirosaki University, 66-1 Honcho, Hirosaki 036-8564, Japan
[j] Shock Wave Research Center, Institute of Fluid Science, Tohoku University, 2-1-1 Katahira, Sendai 980-8577, Japan
[k] Department of Applied Physics, Faculty of Engineering, Tohoku Gakuin University, 1-13-1 Chuo, Tagajo 985-8537, Japan

ABSTRACT

Quasi-monochromatic parallel flash radiography system utilizing a plane-focus plasma x-ray tube in conjunction with an x-ray lens is described. The x-ray generator employs a high-voltage power supply, a low-impedance coaxial transmission line, a high-voltage condenser with a capacity of about 200 nF, a turbo-molecular pump, a krytron pulse generator as a trigger device, and a flash x-ray tube. The high-voltage main condenser is charged up to 50 kV by the power supply, and the electric charges in the condenser are discharged to the tube after triggering the cathode electrode. The flash x-rays are then produced. The x-ray tube is of a demountable triode that is connected to the turbo molecular pump with a pressure of approximately 1 mPa. As the electron flows from the cathode electrode are roughly converged to the target plane by the electric field in the tube, the weakly ionized plasma x-ray source, which consists of copper ions and electrons, forms by the target evaporating. Both the tube voltage and current displayed damped oscillations, and their peak values increased according to increases in the charging voltage. In the present work, the peak tube voltage was almost equal to the initial charging voltage of the main condenser, and the peak current was about 20 kA with a charging voltage of 50 kV. The dimension of x-ray source was almost equal to the target diameter of about 10 mm, and the x-ray pulse widths were less than 1 μs. When the charging voltage was increased, the plasma x-ray source formed, and the characteristic x-ray intensities of K-series lines substantially increased. The quasi-monochromatic x-rays from the plane-focus tube were formed into parallel beam by a polycapillary plate with a hole diameter and a thickness of 25 μm and 1.0 mm, respectively, and quasi-monochromatic radiography was performed by a film-less computed radiography system.

Keywords: Flash x-ray, Quasi-monochromatic radiography, Parallel radiography, X-ray lens, Polycapillary plate

25th International Congress on High-Speed Photography and Photonics,
Claude Cavailler, Graham P. Haddleton, Manfred Hugenschmidt, Editors,
SPIE Vol. 4948 (2003) © 2003 SPIE · 0277-786X/03/$15.00

1. INTRODUCTION

The flash x-ray generator is one of the most powerful tools for performing high-speed radiography in various fields, and a wide variety of generators[1] with x-ray qualities ranging from very soft to hard have been developed corresponding to the radiographic objectives. In particular, because the soft generators[2-8] with photon energies of less than 150 keV can be applied to perform biomedical radiography, we have developed several different generators and have measured distinctive radiographic characteristics.

When it comes to spectrum distribution, the condenser-discharge flash x-ray generator produces soft components as compared with a conventional generator utilizing a hot-cathode x-ray tube, since the discharge current maximizes with decreases in the tube voltage. When the current increases, the plasma forms from the targets evaporation, and intense K-series characteristic x-rays are produced.

Currently, monochromatic parallel radiography has been performed using a synchrotron equipped with monochromators, and it has enabled various researches. In biomedical applications, micro angiography[9] and phase-contrast radiography[10] are remarkable results, and possible further applications have been considered for a long time. However, it is very difficult to obtain sufficient machine times for certain research.

When flash radiography using monochromators is employed, it is not easy to obtain sufficient x-ray intensity for radiography and to increase the dimension of the irradiation field. With recent advances in x-ray optics, several different lenses have been developed, and a low-priced parallel flash radiography system can be realized when a polycapillary plate[11,12] is employed. In addition, a plane-focus tube is needed to increase the dimension of the parallel irradiation field, because the critical angles of total internal reflection are very small.

In this article, we performed tentative study on quasi-monochromatic parallel radiography using a polycapillary plate in conjunction with a plasma x-ray generator utilizing a plane-focus radiation tube.

2. GENERATOR

2.1. High-Voltage Circuit

Figure 1 shows block diagram of a high-intensity plasma flash x-ray generator. This generator consists of the following essential components: a high-voltage power supply, a high-voltage condenser with a capacity of about 200 nF, a turbo-molecular pump, a krytron pulse generator as a trigger device, and a flash x-ray tube. In this generator, a low-impedance transmission line is employed in order to increase maximum tube current. The high-voltage main condenser is charged up to 50 kV by the power supply, and electric charges in the condenser are discharged to the tube after triggering the cathode electrode by the trigger device. The plasma flash x-rays are then produced.

2.2. X-ray Tube

The x-ray tube is of a demountable cold-cathode triode that is connected to the turbo molecular pump with a pressure of approximately 1 mPa (Figure 2). This tube consists of the following major parts: a pipe-shaped carbon cathode with a bore diameter of 10.0 mm, a trigger electrode made from a copper wire, a stainless-steel vacuum chamber, a nylon insulator, a polyethylene terephthalate (Mylar) x-ray window of 0.25 mm, and a disk-shaped copper target of 10.0 mm in diameter. The distance between the anode and cathode electrodes is approximately 10 mm, and the trigger electrode is set in the cathode electrode. As electron beams from the cathode electrode are roughly converged to the target by electric field in the tube, the weakly ionized linear plasma, which consists of copper ions and electrons, forms around the target by evaporating.

2.3. Principle of Characteristic X-ray Irradiation

The plasma grows according to increases in the charging voltage at the tip of the target, and the bremsstrahlung spectra with photon energies of higher than K-absorption edge are absorbed and are converted into fluorescent x-rays. Next, the plasma transmits the fluorescent rays easily, and bremsstrahlung rays with energies of lower than K-edge are also absorbed by the plasma. In addition, because the bremsstrahlung x-rays are hardly produced from the electron accelerating direction due to the angle dependence, intense characteristic x-rays are generated from the plasma.

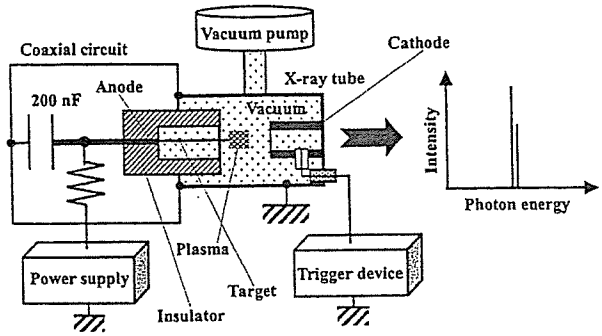

Figure 1. Block diagram of the high-intensity plasma flash x-ray generator.

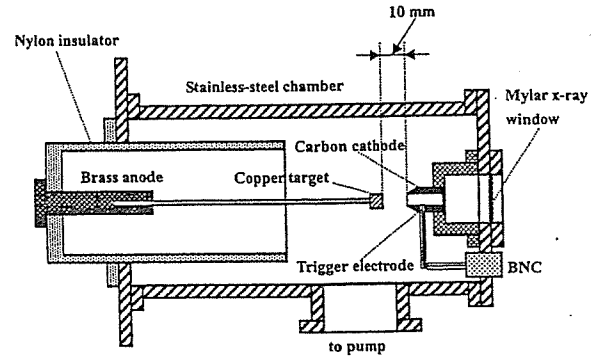

Figure 2. Schematic drawing of the flash x-ray tube with a disk target.

3. CHARACTERISTICS

3.1. Tube Voltage and Current

Tube voltage and current were measured by a high-voltage divider with an input impedance of 1 GΩ and a current transformer, respectively. Figure 3 shows time relation between the tube voltage and current. At the indicated charging voltages, they roughly displayed damped oscillations. When the charging voltage was increased, both the maximum tube voltage and current increased. At a charging voltage of 50 kV, the maximum tube voltage was almost equal to the charging voltage of the main condenser, and the maximum tube current was about 20 kA.

3.2. X-ray Output

X-ray output pulse was detected using a combination of a plastic scintillator and a photomultiplier (Figure 4). The x-ray pulse height substantially increased with corresponding increases in the charging voltage and decreased in the case where a monochromatic copper filter of 10 μm was inserted. The x-ray pulse widths were less than 1 μs, and the time-integrated x-ray intensity measured by a thermoluminescence dosimeter (Kyokko TLD Reader 1500 having MSO-S elements without energy compensation) had a value of about 25 μC/kg at 1.0 m from the x-ray source with a charging voltage of 50 kV.

3.3. X-ray Source

In order to measure images of the plasma x-ray source, we employed a pinhole camera with a hole diameter of 100 μm (Figure 5). When the charging voltage was increased, the plasma x-ray source grew, and both spot dimension and intensity increased. In contrast, both the dimension and intensity decreased according to insertion of the monochromatic filter.

3.4. X-ray Spectra

X-ray spectra from the plasma source were measured by a transmission-type spectrometer with a lithium fluoride curved crystal of 0.5 mm in thickness. The spectra were taken by a computed radiography (CR) system[13] having a wide dynamic range, and relative x-ray intensity was calculated from Dicom digital data. Figure 6 shows measured spectra from the copper target. In fact, we observed quite intense lines of K-series characteristic x-rays and hardly detected bremsstrahlung rays. The characteristic x-ray intensity substantially increased with corresponding increases in the charging voltage and decreased with insertion of the filter.

3.5. X-ray Diffusion by Slits

The intense and sharp characteristic x-rays from the weakly ionized plasma were diffracted and diffused after passing through two lead slits as compared with incoherent x-rays from a conventional x-ray generator, and we have investigated these distinctive phenomena. For this research, in order to measure difference of characteristics between

the incoherent and plasma x-rays, we employed two lead slits in order to measure the diffraction power of characteristic x-rays (Figure 7). Although the characteristic x-rays from the linear plasma are diffused greatly after passing through two slits, these rays were not so diffused as compared to incoherent x-rays.

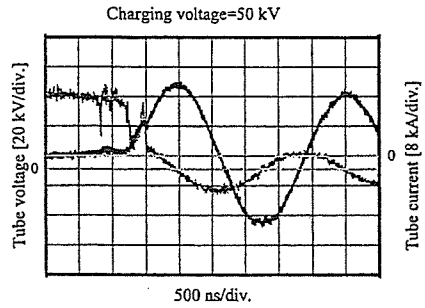

Figure 3. Tube voltages and currents with a charging voltage of 50 kV.

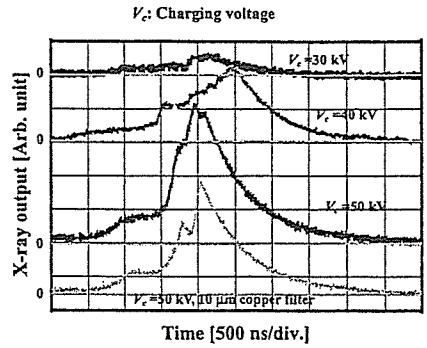

Figure 4. X-ray outputs at the indicated conditions.

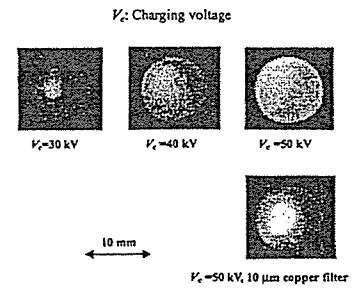

Figure 5. Images of the plasma x-ray source.

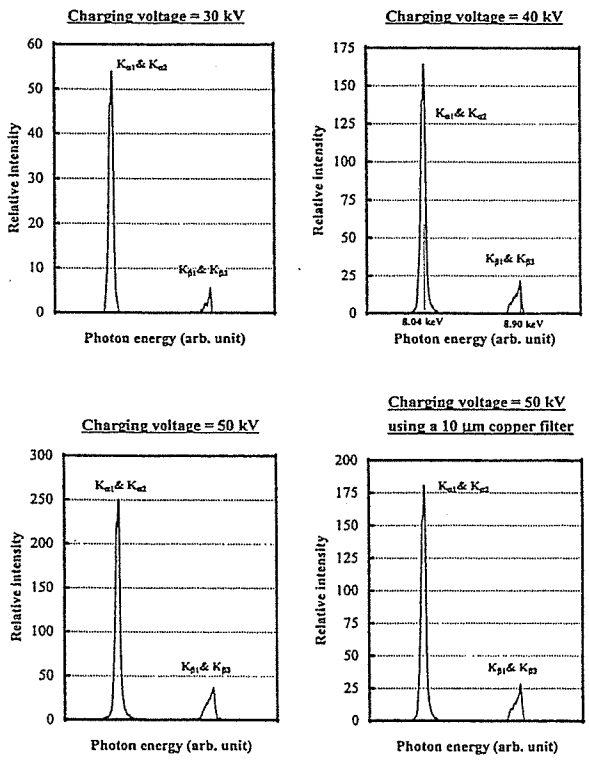

Figure 6. X-ray spectra from the copper-plasma target at the indicated conditions.

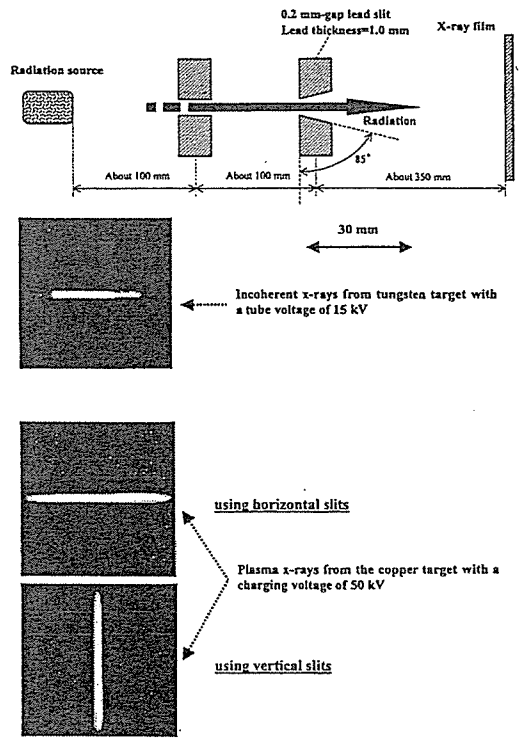

Figure 7. X-ray diffraction by two lead slits.

4. RADIOGRAPHY

The plasma radiography was performed by the CR system, and the charging voltage and the distance between the x-ray source and imaging plate were 50 kV and 1.2 m, respectively.

Figure 8 shows radiograms of a polycapillary plate, and the center of the black spot is almost imaged by the direct transmission beams through capillary holes. After the density control, the spot dimension increases, and the irradiation field increases according to increases in the target diameter and a distance between the x-ray source and the imaging plate. Next, an enlarged radiogram of a test chart for measuring image resolution is shown in Figure 9. In the CR

radiography, the resolution had a value of about 100 μm, and the resolution was almost equal to the CR resolution. Radiograms of a vertebra are shown in Figure 10, and the spatial resolution slightly increased using a polycapillary. Figure 11 shows angiograms of a uterus extracted from a rat using barium-based contrast medium, and fine blood vessels are visible.

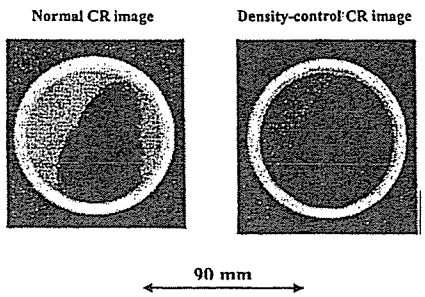

Figure 8. Radiograms of a polycapillary plate

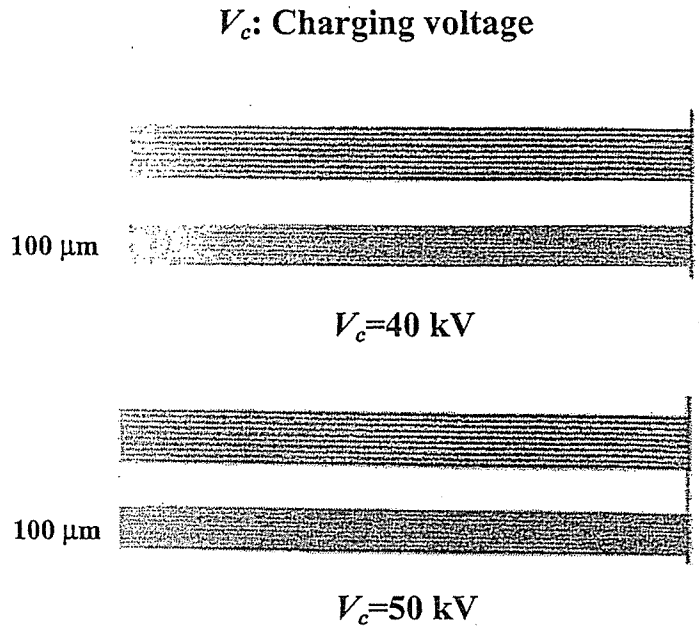

Figure 9. Radiograms of a test chart for measuring image resolution.

Figure 10. Radiograms of a vertebra.

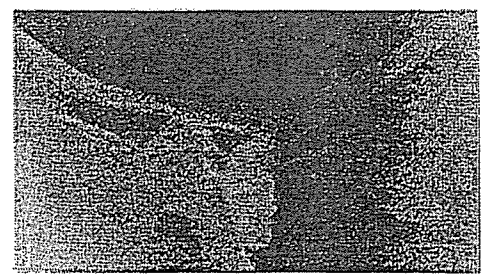

Figure 11. Angiogram of a uterus.

5. DISCUSSION

In the present work, although we have obtained quite intense characteristic x-rays, K_α and K_β lines were not so sharp as compared with those obtained from the axial direction of the weakly ionized linear copper plasma. Next, the beams are not diffused greatly after passing through two lead slits.

In order to simplify equations, we assume that the linear absorption coefficients of K-series characteristic x-rays are almost constant. We assume that the incident angle for reflection in the capillary hole is constant, because the reflecting intensity is approximated, the x-ray intensity without absorbing I_0, transmission intensity I_t, the reflecting intensity I_r, and the intensity for parallel radiography I may be given by:

$$I_0 = K_1 \cdot I_k , \qquad (1)$$

$$I_t \cong K_2 \cdot I_k \cdot \exp(-\mu_c \cdot b), \quad (2)$$

$$I_r \cong K_3 \cdot I_k \cdot R^n, \quad (3)$$

$$I \cong I_0 + I_r >> I_t, \quad (4)$$

where I_k is the incident K-series characteristic x-ray intensity, μ_c is the linear absorption coefficient of a capillary glass, R is the reflecting power ($1 \geqq R \geqq 0$), b is the capillary thickness, and K_1~K_3 are constants.

Using this plasma x-ray generator having a plane-focus x-ray tube, we have obtained sufficient x-ray intensities per pulse for the CR radiography. However, in order to obtain higher intensity, the condenser capacity should be increased as large as possible. Because we are designing a new x-ray lens for high photon energy parallel radiography, this parallel radiography system will perform high-resolution and high-contrast radiography in various fields.

ACKOWLEDGEMENTS

This work was supported by Grants-in-Aid for Scientific Research (12670902, 13470154 and 13877114) from MECSST, Test of Fostering Potential of Japan Science and Technology Corporation, New Energy and Industrial Technology Development Organization, and Cardiovascular Disease (H13C-1) from MHLW.

REFERENCES

1. R. Germer, "X-ray flash techniques," *J. Phys. E: Sci. Instrum.*, **12**, pp. 336-350, 1979.

2. E. Sato, S. Kimura, S. Kawasaki, H. Isobe, K. Takahashi, Y. Tamakawa and T. Yanagisawa, "Repetitive flash x-ray generator utilizing a simple diode with a new type of energy-selective function," *Rev. Sci. Instrum.*, **61**, pp. 2343-2348, 1990.

3. E. Sato, K. Takahashi, M. Sagae, S. Kimura, T. Oizumi, Y. Hayasi, Y. Tamakawa and T. Yanagisawa, "Sub-kilohertz flash x-ray generator utilizing a glass-enclosed cold-cathode triode," *Med. & Biol. Eng. & Comput.*, **32**, pp. 289-294, 1994.

4. K. Takahashi, E. Sato, M. Sagae, T. Oizumi, Y. Tamakawa and T. Yanagisawa, "Fundamental study on a long-duration flash x-ray generator with a surface-discharge triode," *Jpn. J. Appl. Phys.*, **33**, pp. 4146-4151, 1994.

5. E. Sato, M. Sagae, A. Shikoda, K. Takahashi, T. Oizumi, M. Yamamoto, A. Takabe, K. Sakamaki, Y. Hayasi, H. Ojima, K. Takayama and Y. Tamakawa, "High-speed soft x-ray techniques," *SPIE*, **2869**, pp. 937-955, 1996.

6. E. Sato, Y. Hayashi, E. Tanaka, H. Mori, T. Kawai, H. Obara, T. Ichimaru, K. Takayama, H. Ido, T. Usuki, K. Sato and Y. Tamakawa, "Polycapillary radiography using a quasi-x-ray laser generator," *SPIE*, **4508**, pp. 176-187, 2001.

7. E. Sato, Y. Suzuki, Y. Hayashi, E. Tanaka, H. Mori, T. Kawai, K. Takayama, H. Ido and Y. Tamakawa, "High-intensity quasi-monochromatic x-ray irradiation from the linear plasma target," *SPIE*, **4505**, pp. 154-164, 2001.

8. E. Sato, Y. Hayasi, E. Tanaka, H. Mori, T. Kawai, T. Usuki, K. Sato, H. Obara, T. Ichimaru, K. Takayama, H. Ido and Y. Tamakawa, "Quasi-monochromatic radiography using a high-intensity quasi-x-ray laser generator," *SPIE*, **4682**, pp. 538-548 2002.

9. H. Mori, K. Hyodo, E. Tanaka, M.U. Mohammed, A. Yamakawa, Y. Shinozaki, H. Nakazawa, Y. Tanaka, T. Sekka, Y. Iwata, S. Honda, K. Umetani, H. Ueki, T. Yokoyama, K. Tanioka, M. Kubota, H. Hosaka, N. Ishizawa and M. Ando, "Small-vessel radiography in situ with monochromatic synchrotoron radiation," *Radiology*, **201**, pp. 173-177, 1996.

10. A. Momose, T. Takeda, Y. Itai and K. Hirano, "Phase-contrast x-ray computed tomography for observing biological soft tissues," *Nature Medicine*, **2(4)**, pp. 473-475, 1996.

11. Q.F. Xiao and S.V. Poturaef, "Polycapillary-based x-ray optics," *Nucl. Instr. Meth. Phys. Res. A*, **347**, pp. 376-383, 1994.

12. E. Sato, H. Toriyabe, Y. Hayasi, E. Tanaka, H. Mori, T. Kawai, T. Usuki, K. Sato, H. Obara, T. Ichimaru, K. Takayama, H. Ido and Y. Tamakawa,"Fundamental study on parallel beam radiography using a polycapillary plate," *SPIE*, **4682**, pp. 298-310, 2002.

13. E. Sato , K. Sato and Y. Tamakawa, "Film-less computed radiography system for high-speed Imaging," *Ann. Rep. Iwate Med. Univ. Lib. Arts and Sci.*, **35**, pp. 13-23, 2000.

Plasma flash x-ray generator (PFXG-02)

Eiichi Sato[a], Rudolf Germer[b], Yasuomi Hayasi[c], Etsuro Tanaka[d], Hidezo Mori[e], Toshiaki Kawai[f], Tatsumi Usuki[g], Koetsu Sato[g], Haruo Obara[h], Masayuki Zuguchi[h], Toshio Ichimaru[i], Hidenori Ojima[j], Kazuyoshi Takayama[j] and Hideaki Ido[k]

[a] Department of Physics, Iwate Medical University, 3-16-1 Honchodori, Morioka 020-0015, Japan
[b] ITP, FHTW FB1 and TU-Berlin, Blankenhainer Str. 9, D 12249 Berlin, Germany
[c] Electrical Engineering, Hachinohe National College of Technology, 16-1 Tamonoki Uwanotai, Hachinohe 039-1104, Japan
[d] Department of Physiology, School of Medicine, Tokai University, Boseidai, Isehara 259-1193, Japan
[e] Department of Cardiac Physiology, National Cardiovascular Center Research Institute, 5-7-1 Fujishirodai, Suita, Osaka 565-8565 Japan
[f] Electron Tube Division #2, Hamamatsu Photonics Inc., 314-5 Shimokanzo, Toyooka Village, Iwata-gun 438-0193, Japan
[g] Toreck Inc., 5-6-20 Tsunashima Higashi, Yokohama 223-0052, Japan
[h] Department of Radiological Technology, College of Medical Science, Tohoku University, 1-1 Seiryocho, Sendai 980-0872, Japan
[i] Department of Radiological Technology, School of Health Sciences, Hirosaki University, 66-1 Honcho, Hirosaki 036-8564, Japan
[j] Shock Wave Research Center, Institute of Fluid Science, Tohoku University, 2-1-1 Katahira, Sendai 980-8577, Japan
[k] Department of Applied Physics, Faculty of Engineering, Tohoku Gakuin University, 1-13-1 Chuo, Tagajo 985-8537, Japan

ABSTRACT

In the plasma flash x-ray generator, high-voltage main condenser of about 200 nF is charged up to 50 kV by a power supply, and electric charges in the condenser are discharged to an x-ray tube after triggering the cathode electrode. The flash x-rays are then produced. The x-ray tube is of a demountable triode that is connected to a turbo molecular pump with a pressure of approximately 1 mPa. As electron flows from the cathode electrode are roughly converged to a rod iron target of 3.0 mm in diameter by electric field in the x-ray tube, the weakly ionized linear plasma, which consists of iron ions and electrons, forms by target evaporating. At a charging voltage of 50 kV, the maximum tube voltage was almost equal to the charging voltage of the main condenser, and the peak current was about 20 kA. When the charging voltage was increased, the linear plasma formed, and the K-series characteristic x-ray intensities increased. The x-ray pulse widths were about 800 ns, and the time-integrated x-ray intensity had a value of about 10 μC/kg at 1.0 m from x-ray source with a charging voltage of 50 kV. The plasma x-rays were diffused after passing through two lead slits.

Keywords: Flash x-ray, Weakly ionized linear plasma, Intense monochromatic x-rays, New x-ray, Diffusive x-ray

1. INTRODUCTION

Flash x-rays are very useful for performing high-speed radiography, and the maximum photon energy has been increased up to about 1 MeV by increasing the stage number of a Marx type high-voltage pulse generator.[1] Next, an induction linear accelerator[2] has been developed, and the photon energy increased up to about 20 MeV in order to perform radiography for detonics.

In the photon energy region of lower than 150 keV, several different generators[3-5] have been developed, the repetitive generators[6-8] have been used to perform multiple-shot and cine radiographies, and the repetition rate has been increased to sub-kilohertz levels.[9] Although we have developed a sub-megahertz stroboscopic x-ray generator, three other types of stroboscopic x-ray generators[10] have already been manufactured.

Recently, soft x-ray lasers[11] have been produced using a gas-discharge capillary, and laser intensity increases with increases in the capillary length. However, it is not easy to increase the photon energy up to about 10 keV or higher using light amplification by stimulated emission. Without considering coherence, we have developed several different plasma flash x-ray generators[12,13] to increase K-series characteristic x-rays by forming weakly ionized linear plasma. In the plasma, bremsstrahlung x-rays with energies of higher than K-absorption edge are absorbed and converted into fluorescent x-rays, and intense characteristic x-rays have been produced by x-ray enhancement of fluorescent x-rays. By forming linear plasma, we have already succeeded in generating intense and sharp quasi-monochromatic x-rays such as laser and have hardly observed bremsstrahlung x-rays. Therefore, we have to measure radiographic characteristics according to changes in the target element of the plasma x-ray tube.

In the present work, we introduce a new plasma flash x-ray generator for generating intense characteristic x-rays, and we have measured radiographic characteristics of weakly ionized linear plasma of iron.

2. GENERATOR

2.1. High-Voltage Circuit

Figure 1 shows block diagram of a high-intensity plasma flash x-ray generator. This generator consists of the following essential components: a high-voltage power supply, a high-voltage condenser with a capacity of about 200 nF, a turbo-molecular pump, a krytron pulse generator as a trigger device, and a flash x-ray tube. In this generator, a low-impedance transmission line is employed in order to increase maximum tube current. The high-voltage main condenser is charged up to 50 kV by the power supply, and electric charges in the condenser are discharged to the tube after triggering the cathode electrode by the trigger device. The plasma flash x-rays are then produced.

2.2. X-ray Tube

The x-ray tube is of a demountable cold-cathode triode that is connected to the turbo molecular pump with a pressure of approximately 1 mPa (Figure 2). This tube consists of the following major parts: a pipe-shaped carbon cathode with a bore diameter of 10.0 mm, a trigger electrode made from a copper wire, a stainless-steel vacuum chamber, a nylon insulator, a polyethylene terephthalate (Mylar) x-ray window of 0.25 mm, and a rod-shaped iron target of 3.0 mm in diameter. The distance between the anode and cathode electrodes is approximately 15 mm, and the trigger electrode is set in the cathode electrode. As electron beams from the cathode electrode are roughly converged to the target by electric field in the tube, the weakly ionized linear plasma, which consists of iron ions and electrons, forms around the fine target by evaporating.

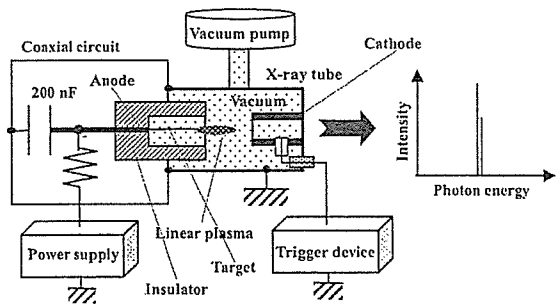

Figure 1. Block diagram of the high-intensity plasma flash x-ray generator.

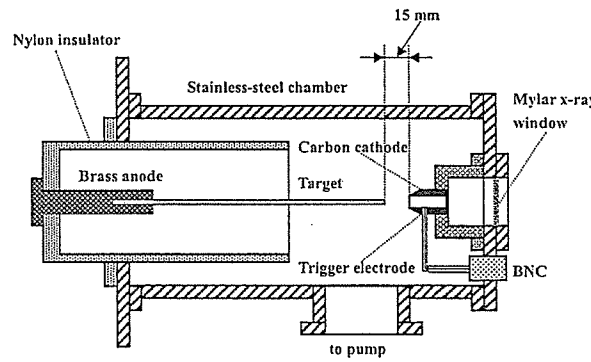

Figure 2. Schematic drawing of the flash x-ray tube with a rod target.

2.3. Principle of Characteristic X-ray Irradiation

If we assume that the thickness of linear plasma has a small value, x-ray spectra from the transverse direction is almost equivalent to standard distribution from a conventional x-ray generator having a hot-cathode tube. In the plasma, bremsstrahlung spectra with photon energies of higher than K-absorption edge are effectively absorbed and are converted into fluorescent x-rays. Next, the plasma transmits the fluorescent rays easily, and bremsstrahlung rays with energies of lower than K-edge are also absorbed by the plasma. In addition, because K-fluorescent yield corresponding to conversion efficiency approaches one according to increases in atomic number, intense characteristic x-rays are

generated from the plasma-axial direction (refer to Figure 1).

3. CHARACTERISTICS

3.1. Tube Voltage and Current

Tube voltage and current were measured by a high-voltage divider with an input impedance of 1 GΩ and a current transformer, respectively. Figure 3 shows time relation between the tube voltage and current. At the indicated charging voltages, they roughly displayed damped oscillations. When the charging voltage was increased, both the maximum tube voltage and current increased. At a charging voltage of 50 kV, the maximum tube voltage was almost equal to the charging voltage of the main condenser, and the maximum tube current was about 20 kA.

3.2. X-ray Output

X-ray output pulse was detected using a combination of a plastic scintillator and a photomultiplier (Figure 4). The x-ray pulse height substantially increased with corresponding increases in the charging voltage. The x-ray pulse widths were about 800 ns, and the time-integrated x-ray intensity measured by a thermoluminescence dosimeter (Kyokko TLD Reader 1500 having MSO-S elements without energy compensation) had a value of about 10 μC/kg at 1.0 m from the x-ray source with a charging voltage of 50 kV.

3.3. X-ray Source

In order to measure images of the plasma x-ray source, we employed a pinhole camera with a hole diameter of 100 μm (Figure 5). When the charging voltage was increased, the plasma x-ray source grew, and both spot dimension and intensity increased

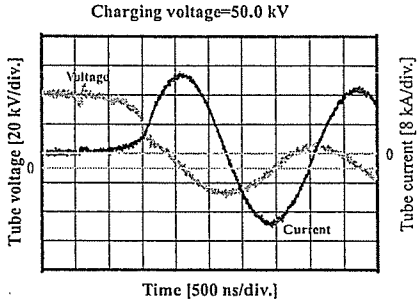

Figure 3. Tube voltages and currents with a charging voltage of 50.0 kV.

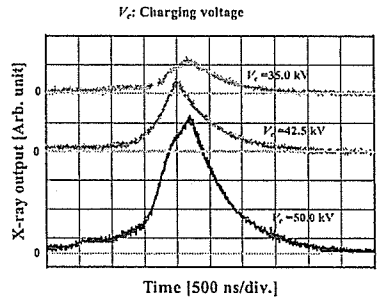

Figure 4. X-ray outputs at the indicated charging voltages.

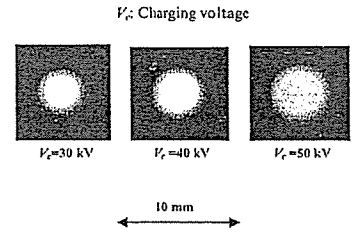

Figure 5. Images of the plasma x-ray source.

3.4. X-ray Spectra

X-ray spectra from the plasma source were measured by a transmission-type spectrometer with a lithium fluoride curved crystal of 0.5 mm in thickness. The spectra were taken by a computed radiography (CR) system[14] having a wide dynamic range, and relative x-ray intensity was calculated from Dicom digital data. Figure 6 shows measured spectra from the iron target. When the transmission-type spectrometer was employed, it was very difficult to detect the K series characteristic x-rays of iron. However, the characteristic x-rays increased with increases in the charging voltage, and $K_{\alpha 1}$ line increased and became to single K_α line. In the iron spectra, we slightly observed bremsstrahlung x-rays at a higher charging voltage. In comparison, we introduce the spectra from the copper target. In fact, we observed quite sharp lines of K-series characteristic x-rays such as lasers and hardly detected bremsstrahlung rays. The characteristic x-ray intensity substantially increased with corresponding increases in the charging voltage.

3.5. X-ray Diffraction by Slits

Although coherence is the most important factor in x-ray amplification, it is quite difficult to measure the coherence, because the x-rays for biomedical radiography can penetrate various objects easily. For this research, in order to

measure difference of characteristics between the incoherent and plasma x-rays, we employed two lead slits in order to measure the diffraction power of characteristic x-rays (Figure 8). As compared with incoherent x-rays from a hot-cathode x-ray tube, the characteristic x-rays from the linear plasma are diffracted and diffused after passing through two slits.

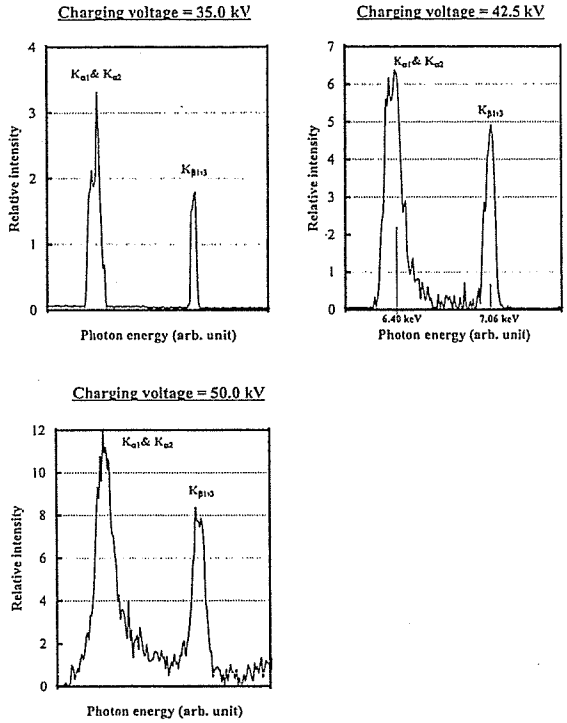

Figure 6. X-ray spectra from the iron-plasma target at the indicated conditions.

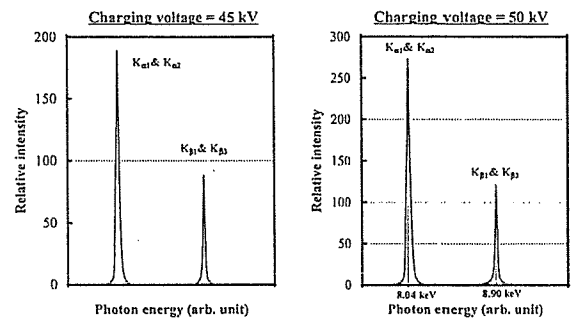

Figure 7. X-ray spectra from the copper-plasma target at the indicated conditions.

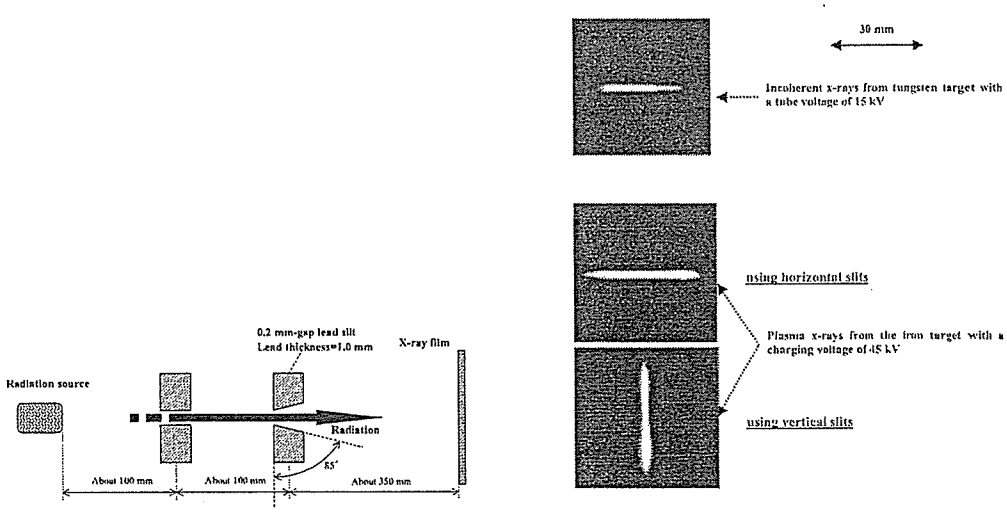

Figure 8. X-ray diffusion by two lead slits.

4. RADIOGRAPHY

The plasma radiography was performed by the CR system, and the charging voltage and the distance between the x-ray source and imaging plate were 45 kV and 1.2 m, respectively.

A radiogram of cigarettes is shown in Figure 9, and the contents of cigarettes were observed vividly. Next,

because the photon energies of the K-series lines of copper ranged from 6.4 to 7.1 keV, we could image a thin film for food wrapping. An angiogram of a uterus extracted from a rat using barium-based contrast medium is shown in Figure 11. In this radiography, we also obtained a soft image and observed finer blood vessels. Figure 12 shows an angiogram of a heart extracted from a rabbit using iodine-based microspheres of 20 μm. Although the characteristic x-rays hardly penetrated the heart, fine blood vessels were comparatively visible.

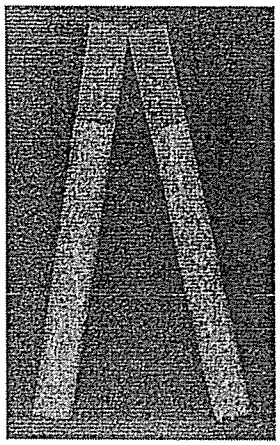

Figure 9. Radiogram of cigarettes.

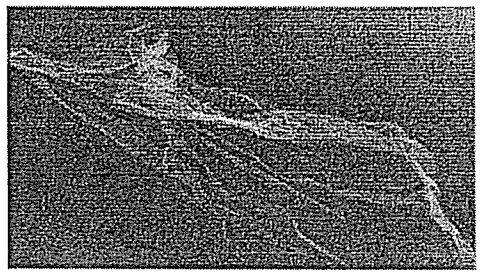

Figure 10. Radiogram of a film.

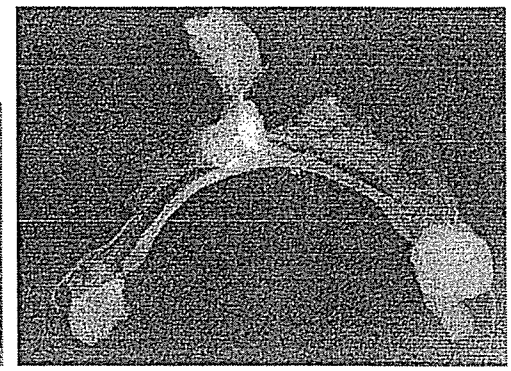

Figure 11. Angiograms of a uterus extracted from a rat.

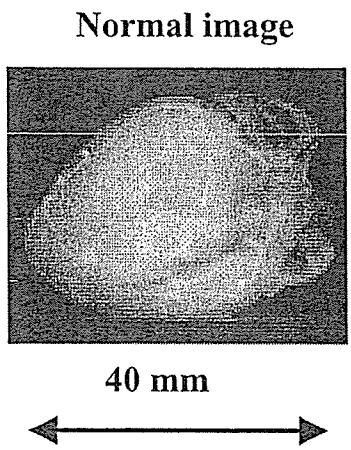

Figure 12. Angiograms of a heart extracted from a rabbit.

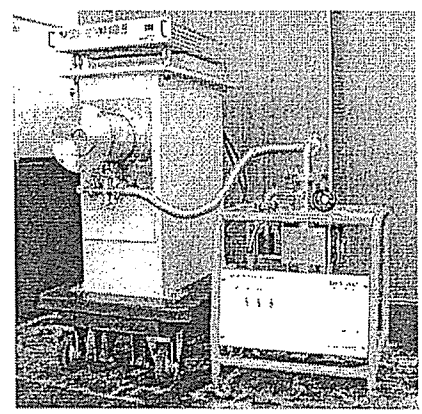

Figure 13. Plasma flash x-ray generator (PFXG-02).

5. DISCUSSION

For this research, we have obtained intense K-series characteristic x-rays, and have performed quite soft quasi-monochromatic radiography. Because it is quite difficult to generate higher-dose-rate x-rays in a lower photon energy region of about 10 keV or lower using a conventional x-ray generator having a hot-cathode tube, it goes without saying that plasma flash x-ray generator has strong power to produce intense and high-dose-rate x-rays.

In this generator, the x-rays are produced from both solid and plasma targets, and the solid target is covered with a plasma cloud. In order to simplify the consideration, if we assume that the solid target is negligible, the K photons are produced from the weakly ionized linear plasma by the fine target evaporation. In this case, the total characteristic x-ray intensity I_k from the plasma is written as:

$$I_k = (na)^{-1} \sum_{i=1}^{n} \{I_k(E_i) + I'_k(E_i)\} \int_0^a \exp\{-\mu_p(E_i) \cdot x\}\, dx, \qquad (1)$$

where E_i is the photon energy of the characteristic x-rays, $I_k(E_i)$ is the converted K-series characteristic x-ray intensity,

$I'_k(E_i)$ is the initial K-series x-ray intensity generated in the plasma, $\mu_p(E_i)$ is the linear absorption coefficient of plasma, a is the plasma length, and x is the plasma depth.

Although accelerated electrons collide with the plasma target from various directions, we employ the simplest model. So as to calculate the number of characteristic K_i photons from the plasma target, if we assume that the maximum photon energy E_0 is a constant to simplify the equation, the photon number N_{ki} is represented by:

$$N_{ki} \cong K\omega_k \int_0^a \int_{Ek}^{E_0} N_e(E, x) \cdot \sigma_k(E) \cdot \exp\{-\mu_p(E_i) \cdot x\}\, dE \quad dx . \qquad (2)$$

Here, ω_k is the K-fluorescent yield, E_k is the critical excitation energy, μ_{ki} is the linear absorption coefficient in the plasma, $\sigma_k(E)$ is the cross section for K-photon radiation in the plasma, $N_e(E,x)$ is the electron distribution at the depth x in the plasma, and K is a constant.

Using this plasma x-ray generator, since the photon energy can be selected by the target element and can be increased up to about 60 keV using a tungsten target, these intense characteristic x-rays without bremsstrahlung rays may be applied to perform quasi-monochromatic or monochromatic high-speed radiography instead of synchrotron.

ACKOWLEDGEMENTS

This work was supported by Grants-in-Aid for Scientific Research (12670902, 13470154 and 13877114) from MECSST, Test of Fostering Potential of Japan Science and Technology Corporation, New Energy and Industrial Technology Development Organization, and Cardiovascular Disease (H13C-1) from MHLW.

REFERENCES

1. R. Germer, "X-ray flash techniques," *J. Phys. E: Sci. Instrum.*, **12**, pp. 336-350, 1979.

2. C. Cavailler, "AIRIX- a new tool for flash radiography in detonics," *SPIE*, **4183**, pp. 23-35, 2000.

3. E. Sato, H. Isobe and F. Hoshino, "High intensity flash x-ray apparatus for biomedical radiography," *Rev. Sci. Instrum.*, **57**, pp.1399-1408, 1986.

4. E. Sato, M. Sagae, K. Takahashi, T. Oizumi, H. Ojima, K. Takayama, Y. Tamakawa, T. Yanagisawa, A. Fujiwara and K. Mitoya, "High-speed soft x-ray generators in biomedicine," *SPIE*, **2513**, pp. 649-667, 1994.

5. E. Sato, M. Sagae, A. Shikoda, K. Takahashi, T. Oizumi, M. Yamamoto, A. Takabe, K. Sakamaki, Y. Hayasi, H. Ojima, K. Takayama and Y. Tamakawa, "High-speed soft x-ray techniques," *SPIE*, **2869**, pp. 937-955, 1996.

6. E. Sato, S. Kimura, S. Kawasaki, H. Isobe, K. Takahashi, Y. Tamakawa and T. Yanagisawa, "Repetitive flash x-ray generator utilizing a simple diode with a new type of energy-selective function," *Rev. Sci. Instrum.*, **61**, pp. 2343-2348, 1990.

7. A. Shikoda, E. Sato, M. Sagae, T. Oizumi, Y. Tamakawa and T. Yanagisawa, "Repetitive flash x-ray generator having a high-durability diode driven by a two-cable-type line pulser," *Rev. Sci. Instrum.*, **65**, pp. 850-856, 1994.

8. K. Takahashi, E. Sato, M. Sagae, T. Oizumi, Y. Tamakawa and T. Yanagisawa, "Fundamental study on a long-duration flash x-ray generator with a surface-discharge triode," *Jpn. J. Appl. Phys.*, **33**, pp. 4146-4151, 1994.

9. E. Sato, K. Takahashi, M. Sagae, S. Kimura, T. Oizumi, Y. Hayasi, Y. Tamakawa and T. Yanagisawa, "Sub-kilohertz flash x-ray generator utilizing a glass-enclosed cold-cathode triode," *Med. & Biol. Eng. & Comput.*, **32**, pp. 289-294, 1994.

10. E. Sato, Y. Hayasi and Y. Tamakawa, "Recent stroboscopic x-ray generators and their applications to high-speed radiography," *Ann. Rep. Iwate Med. Univ. Lib. Arts and Sci.*, **35**, pp. 1-11, 2000.

11. J.J.G. Rocca, J.L.A. Chilla, S. Sakadzic, A. Rahman, J. Filevich, E. Jankowska, E.C. Hammarsten, B.M. Luther, H.C. Kapteyn, M. Murnane and V.N. Shlyapsev, "Advances in capillary discharge soft x-ray laser research," *SPIE*, **4505**, pp. 1-6 2001.

12. E. Sato, Y. Hayashi, E. Tanaka, H. Mori, T. Kawai, H. Obara, T. Ichimaru, K. Takayama, H. Ido, T. Usuki, K. Sato and Y. Tamakawa, "Polycapillary radiography using a quasi-x-ray laser generator," *SPIE*, **4508**, pp. 176-187, 2001.

13. E. Sato, Y. Hayasi, E. Tanaka, H. Mori, T. Kawai, T. Usuki, K. Sato, H. Obara, T. Ichimaru, K. Takayama, H. Ido and Y. Tamakawa, "Quasi-monochromatic radiography using a high-intensity quasi-x-ray laser generator," *SPIE*, **4682**, pp. 538-548 2002.

14. E. Sato , K. Sato and Y. Tamakawa, "Film-less computed radiography system for high-speed Imaging," *Ann. Rep. Iwate Med. Univ. Lib. Arts and Sci.*, **35**, pp. 13-23, 2000.

[論　文]

Intense Characteristic X-ray Irradiation from Weakly Ionized Linear Plasma and Applications

Eiichi SATO, Yasuomi HAYASI[†], Rudolf GERMER[††], Etsuro TANAKA[†††], Hidezo MORI[††††], Toshiaki KAWAI[†††††], Haruo OBARA[††††††], Toshio ICHIMARU[†††††††], Kazuyoshi TAKAYAMA[††††††††] and Hideaki IDO[†††††††††]

Department of Physics, Iwate Medical University, 3-16-1 Honchodori, Morioka 020-0015, Japan
[†]Department of Electrical Engineering, Hachinohe National College of Technology, 16-1 Tamonoki Uwanotai, Hachinohe 039-1104, Japan
[††]ITP, FHTW FB1 and TU-Berlin, Blankenhainer Str. 9, D 12249 Berlin, Germany
[†††]Department of Physiology, School of Medicine, Tokai University, Boseidai, Isehara 259-1193, Japan
[††††]Department of Cardiac Physiology, National Cardiovascular Center Research Institute, 5-7-1 Fujishiro-dai, Suita, Osaka 565-8565, Japan
[†††††]Electron Tube Division #2, Hamamatsu Photonics Inc., 314-5 Shimokanzo, Toyooka Village, Iwata-gun 438-0193, Japan
[††††††]Department of Radiological Technology, College of Medical Science, Tohoku University, 1-1 Seiryocho, Sendai 980-0872, Japan
[†††††††]Department of Radiological Technology, School of Health Sciences, Hirosaki University, 66-1 Honcho, Hirosaki 036-8564, Japan
[††††††††]Shock Wave Research Center, Institute of Fluid Science, Tohoku University, 2-1-1 katahira, Aoba-ku, Sendai 980-8577, Japan
[†††††††††]Department of Applied Physics, Faculty of Engineering, Tohoku Gakuin University, 1-13-1 Chuo, Tagajo 985-0873, Japan
(Received June 9, 2002, in final form, April 28, 2003)

Abstract : In the plasma flash x-ray generator, a high-voltage main condenser of approximately 200 nF is charged up to 55 kV by a power supply, and electric charges in the condenser are discharged to an x-ray tube after triggering the cathode electrode. The flash x-rays are then produced. The x-ray tube is a demountable triode that is connected to a turbo molecular pump with a pressure of approximately 1 mPa. As electron flows from the cathode electrode are roughly converged to a rod target by electric field in the x-ray tube, the weakly ionized linear plasma, which consists of molybdenum ions and electrons, forms by target evaporation. At a charging voltage of 50 kV, the maximum tube voltage was almost equal to the charging voltage of the main condenser, and the peak current was about 20 kA. When the charging voltage was increased, the linear plasma formed, and the K -series characteristic x-ray intensities increased. The K lines were quite sharp and intense, and hardly any bremsstrahlung rays were detected. When a copper target was employed, the x-ray pulse widths were approximately 700 ns, and the time-integrated x-ray intensity had a value of approximately 30 μC/kg at 1.0 m from the x-ray source with a charging voltage of 50 kV.

Key words : flash x-ray, characteristic x-ray, quasi-monochromatic x-ray, weakly ionized plasma, linear plasma, micro-angiography.

1. INTRODUCTION

Synchrotrons generate high-dose-rate monochromatic x-rays utilizing silicon monochromators, and the x-ray photon energy is determined by Bragg's angle. These rays play an important role in parallel radiography and

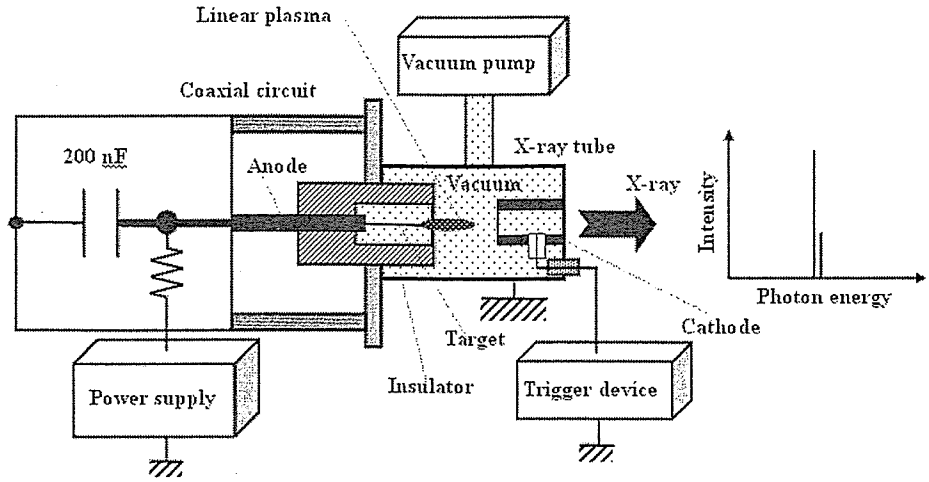

Fig. 1 Block diagram of the high-intensity plasma flash x-ray generator.

have been employed to perform microangiography [1] and phase imaging [2,3]. However, the synchrotrons consume high energies, and it is difficult to obtain sufficient machine times for medical diagnosis and other applications.

Currently, flash x-ray generators utilize cold-cathode radiation tubes and produce high-dose-rate x-rays [4-12]. Therefore, in order to produce fairly high-dose-rate monochromatic x-rays in a small laboratory, plasma flash x-ray generators are useful. Subsequently, we confirmed the irradiation of intense characteristic x-rays from the plasma axial direction using plate targets. Thereafter, we developed a new plasma flash x-ray tube with a rod-shaped target [15,16], and confirmed fairly intense and sharp characteristic x-rays such as lasers from weakly ionized linear plasma.

Photon energies of characteristic x-rays are determined by the target element, and characteristic x-rays from a cerium target are useful to perform angiography using an iodine-based contrast medium, since the photon energies of K-series lines of cerium are slightly higher than the energy of the K-absorption edge of iodine. On the other hand, cerium is a rare earth element and has a high reactivity, and it is difficult to design the target. However, the development of a cerium plasma tube for high-contrast angiography has long been wished for.

In this paper, we describe a singe flash x-ray generator for producing intense characteristic x-rays by forming weakly ionized linear plasma, used to perform quasi-monochromatic radiography.

2. GENERATOR

2.1 High-voltage circuit

Figure 1 shows a block diagram of a high-intensity plasma flash x-ray generator. This generator consists of the following essential components : a high-voltage power supply, a high-voltage condenser with a capacity of approximately 200 nF, a turbo-molecular pump, a krytron pulse generator as a trigger device, and a flash x-ray tube. In this generator, a low-impedance transmission line is employed in order to increase maximum tube current. The high-voltage main condenser is charged up to 55 kV by the power supply, and electric charges in the condenser are discharged to the tube after triggering the cathode electrode with the trigger device. The plasma flash x-rays are then produced.

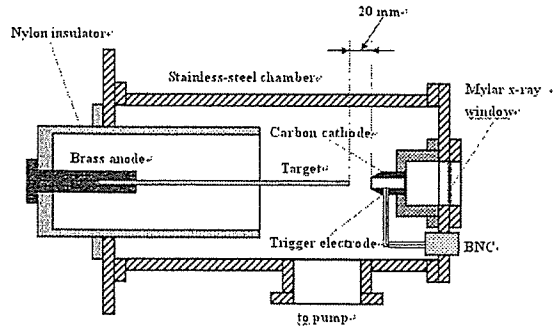

Fig. 2 Schematic drawing of the flash x-ray tube with a rod target.

2.2 X-ray tube

The x-ray tube is a demountable cold cathode triode that is connected to the turbo molecular pump with a pressure of approximately 1 mPa (Fig. 2). This tube consists of the following major parts : a pipe-shaped carbon cathode with a bore diameter of 10.0 mm, a trigger electrode made from copper wire, a stainless-steel vacuum chamber, a nylon insulator, a polyethylene terephthalate (Mylar) x-ray window of 0.25 mm in thickness, and a rod-shaped targets made of copper, molybdenum, and cerium. The diameters of copper, molybdenum, and cerium targets are 3.0, 2.0, and 3.0 mm, respectively. The distance between the target and cathode electrodes is approximately 20 mm, and the trigger electrode is set in the cathode electrode. As electron beams from the cathode electrode are roughly converged to the target by the electric field in the tube, evaporation leads to the formation of weakly ionized linear plasma, consisting of molybdenum ions and electrons, around the fine target.

2.3 Principle of characteristic x-ray irradiation

In the linear plasma, bremsstrahlung spectra with photon energies of higher than the K-absorption edge are effectively absorbed and are converted into fluorescent x-rays (Fig. 3). The plasma transmits the fluorescent rays easily, and bremsstrahlung rays with energies of lower than the K-edge are also absorbed by the plasma. In addition, because bremsstrahlung rays are not emitted in the direction opposite to electron acceleration, intense characteristic x-rays are generated from the plasma-axial direction.

3. CHARACTERISTICS

3.1 Tube voltage and current

Tube voltage and current were measured by a high-voltage divider with an input impedance of 1 GΩ and a current transformer, respectively. Figure 4 shows the time relation between the tube voltage and current obtained using a copper target. At the indicated charging voltages, they roughly displayed damped oscillations. When the charging voltage was increased, both the maximum tube voltage and current increased. At a

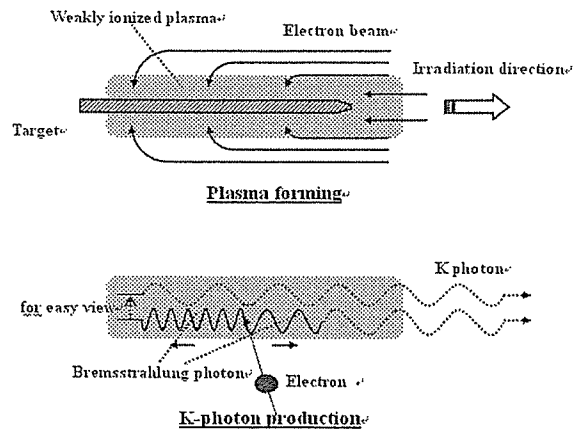

Fig. 3 K-photon irradiation from the plasma.

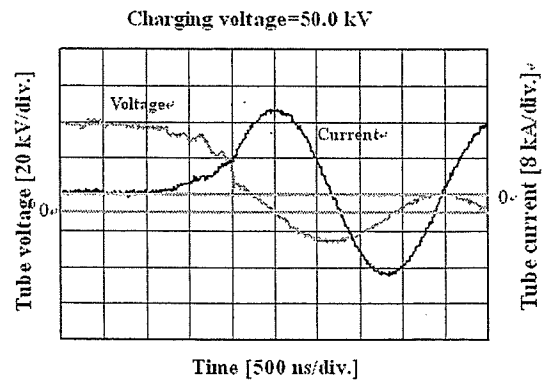

Fig. 4 Tube voltage and current obtained by a copper target with a charging voltage 50 kV.

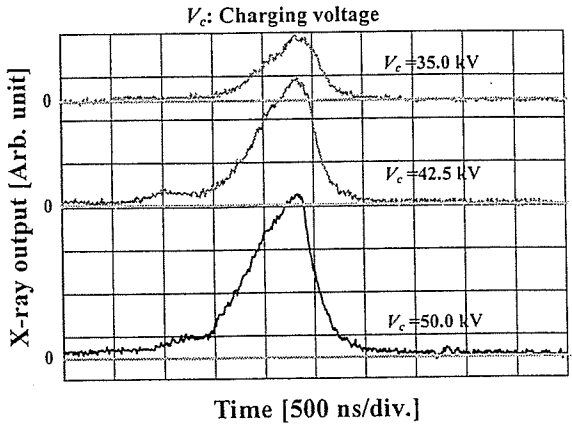

Fig. 5 X-ray outputs using a copper target.

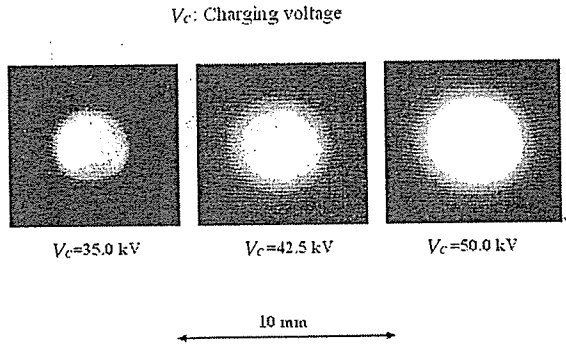

Fig. 6 Images of copper plasma x-ray source.

charging voltage of 50 kV, the maximum tube voltage was almost equal to the charging voltage of the main condenser, and the maximum tube current was approximately 20 kA.

3.2 X-ray output

X-ray output pulse was detected using a combination of a plastic scintillator and a photomultiplier. The x-ray pulse height substantially increased with corresponding increases in the charging voltage when the copper target was employed (Fig. 5). The x-ray pulse widths were about 700 ns, and the time-integrated x-ray intensity measured by a thermoluminescence dosimeter (Kyokko TLD Reader 1500 having MSO-S elements without energy compensation) had a value of about 30 μC/kg at 1.0 m from the x-ray source with a charging voltage of 50 kV.

3.3 X-ray source

In order to measure images of copper plasma x-ray source, we employed a pinhole camera with a hole diameter of 100 μm (Fig. 6). When the charging voltage was increased, the plasma x-ray source grew, and both

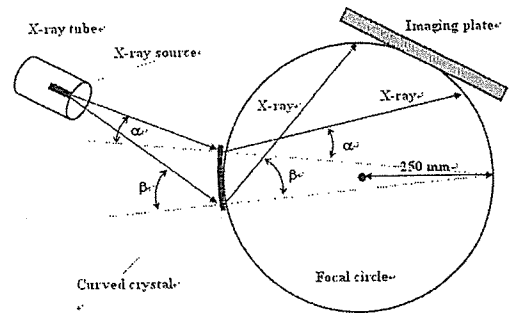

Fig. 7 Transmission-type spectrometer using an imaging plate.

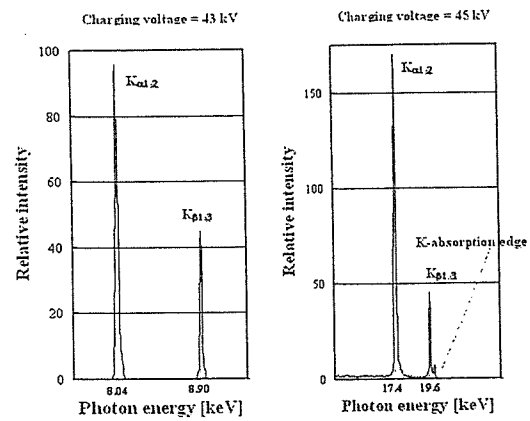

Fig. 8 X-ray spectra from weakly ionized copper and molybdenum plasmas.

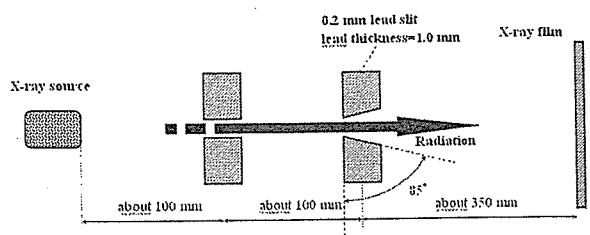

Fig. 9 Experimental setup for measuring x-ray divergence using two lead slits.

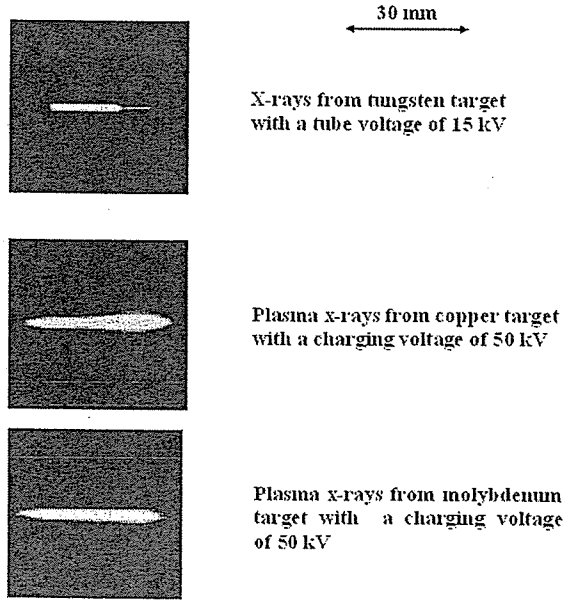

Fig. 10 X-ray divergence using copper and molybdenum targets.

spot dimension and intensity increased. In contrast, both the dimension and intensity decreased according to insertion of the monochromatic filter.

3.4 X-ray spectra

X-ray spectra from the plasma source were measured by a transmission-type spectrometer with a lithium fluoride curved crystal of 0.5 mm in thickness (Fig. 7). The spectra were taken by a computed radiography (CR) system [17] with a wide dynamic range, and relative x-ray intensity was calculated from DICOM digital data. Figure 8 shows measured spectra from the copper and the molybdenum targets. In fact, we observed quite sharp lines of K-series characteristic x-rays such as lasers, while bremsstrahlung rays were hardly detected. The characteristic x-ray intensity substantially increased with corresponding increases in the charging voltage and decreased with insertion of the filter.

3.5 X-ray diffraction by slits

In order to measure the difference in characteristics between x-rays from a conventional tube and these from the plasma tubes, we employed two lead slits in order to measure the divergence of the x-rays (Fig. 9). As compared with x-rays from a conventional tube with a tungsten target, the characteristic x-rays from linear plasmas of copper and molybdenum were diffused greatly after passing through the two slits (Fig. 10).

4. RADIOGRAPHY

The plasma radiography was performed by the CR system (Konica Regius 150) without using a monochromatic filter, and the distance between the x-ray source and imaging plate was 1.2 m. Radiograms

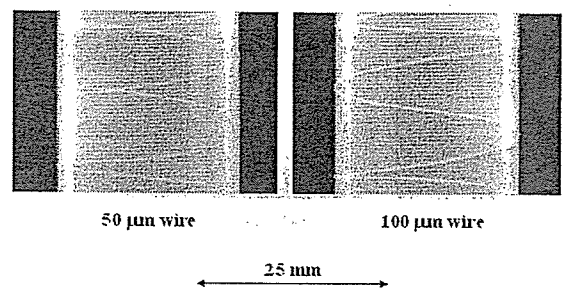

Fig. 11 Radiograms of tungsten wires 50 and 100 μm in diameter, respectively, coiled around pipes made of PMMA

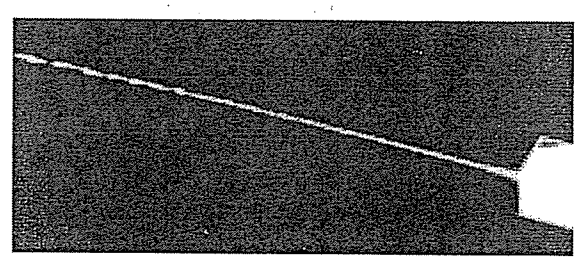

Fig. 12 Radiogram of water spouted from an injector.

Table 1 K-series characteristic x-rays of copper.

Line	Relative intensity	Photon energy (keV)
$K_{\alpha 1}$	100	8.046
$K_{\alpha 2}$	50	8.026
$K_{\alpha 1,2}$	150	8.040
$K_{\beta 1}$	6	8.901
$K_{\beta 1,3}$	20	8.904